Nanosphere Lithography: Fabrication of Large-Area Ag Nanoparticle Arrays by Convective Self-Assembly and Their Characterization by Scanning UV−Visible Extinction Spectroscopy

Anjeanette D. Ormonde,[†] Erin C. M. Hicks,[‡] Jimmy Castillo,[§] and Richard P. Van Duyne*,[‡]

Chemistry Department, Northwestern University, 2145 Sheridan Road, Evanston, Illinois 60208, Facultad de Ciencias, Escuela de Quimica, P.O. Box 47102, Caracas, 1020A Venezuela, and Unilever HPC-USA, Rolling Meadows, Illinois 60008

Received March 1, 2004. In Final Form: May 14, 2004

This work employs UV−visible extinction spectroscopy as a new spectral mapping technique to characterize self-assembled polystyrene microsphere samples produced by convective self-assembly (CSA). This spectroscopic technique was successfully used to analyze the periodic particle arrays produced by the polystyrene template, yielding a detailed characterization of each sample. The CSA-prepared samples proved to be more uniform across a sample as well as more reproducible than previous sample preparation techniques. For the first time, a detailed characterization and quantitative evaluation of the entire sample has been performed by spectroscopic mapping.

Introduction

The study of nanomaterials and their size-dependent properties is a fast growing field of research. This interest has largely been driven by the need for smaller, cheaper, and faster devices in a wide range of industries from microelectronics to medicine.[1] In recent years, much of nanoscience research has been focused on the study of metal nanoparticles. Metal nanoparticles show evidence of not only unique catalytic,[2,3] electronic,[4,5] and magnetic[6,7] properties but also distinctive optical properties that depend on their size, shape and metal composition and the refractive index of the surroundings. Previous research has shown that tuning of the localized surface plasmon resonance (LSPR) of Au and Ag[8] nanoparticles fabricated by nanosphere lithography (NSL)[9−12] is possible throughout the visible and infrared region of the electromagnetic spectrum.[13,14] When metal nanoparticles are excited by electromagnetic radiation, they exhibit collective oscillations of the conduction electrons known as localized surface plasmons. The wavelength corresponding to the extinction maximum, λ_{max}, of the LSPR is highly dependent on the structure and surroundings of the metal nanoparticles.[15,16] The primary assets of LSPR excitation are selective photon absorption, scattering, and local electromagnetic field enhancement. The ability to manipulate and predict the LSPR of metal nanoparticle systems is desirable in several technological applications. For example, these arrays have been used as chemical and biological sensors by monitoring the shift in the LSPR λ_{max} as binding events occur, causing changes in the local refractive index.[17]

To utilize these arrays, various methods of sample preparation have been developed. These include employing angled cooling plates,[18,19] template-directed growth,[20] field-induced growth,[21,22] Langmuir−Blodgett techniques,[23] and the drop-coat technique previously used for NSL.[10,15,16] Unfortunately, each technique suffers from its own limitations, such as requirements of expensive equipment, difficult implementation, little control over packing morphologies, inconsistencies in sample reproducibility, or applicability to a limited selection of substrate materials. In addition, there is no quantitative method to characterize the effectiveness of the samples produced by these techniques over large areas.

Even though NSL is only applicable to a few substrate materials, it provides outstanding control of nanoparticle

* To whom correspondence should be addressed. E-mail: vanduyne@chem.northwestern.edu.
[†] Unilever HPC-USA.
[‡] Northwestern University.
[§] Escuela de Quimica.

(1) Turner, A. P. F. *Science* **2000**, *290*, 1315.
(2) Mascini, M.; Palchetti, I.; Marazza, G. *Anal. Chem.* **2001**, *369*, 15.
(3) Thevenot, D. R.; Toth, K.; Durst, R. A.; Wilson, G. S. *Biosens. Bioelectron.* **2001**, *16*, 121.
(4) Horacek, J.; Skladal, P. *Anal. Chim. Acta* **1997**, *347*, 43.
(5) Ebersole, R. C.; Miller, J. A.; Moran, J. R.; Ward, M. D. *J. Am. Chem. Soc.* **1990**, *112*, 3239.
(6) Miller, M. M.; Sheehan, P. E.; Edelstein, R. L.; Tamanaha, C. R.; Ahong, L.; Bounnak, S.; Whitman, L. J.; Colton, R. J. *J. Magn. Magn. Mater.* **2001**, *225*, 156.
(7) Chemla, Y. R.; Grossman, H. L.; Poon, Y.; McDermott, R.; Stevens, R.; Alper, M. D.; Clarke, J. *Proc. Natl. Acad. Sci. U.S.A.* **2000**, *97*, 26.
(8) Duval Malinsky, M.; Kelly, L.; Schatz, G. C.; Van Duyne, R. P. *J. Am. Chem. Soc.* **2001**, *123*, 1474.
(9) Frey, W.; Woods, C. K.; Chilkoti, A. *Adv. Mater.* **2000**, *12*, 1515.
(10) Hulteen, J. C.; Van Duyne, R. P. *J. Vac. Sci. Technol.* **1995**, *13*, 1553.
(11) Bartlett, P. N.; Birkin, P. R.; Ghanem, M. A. *Chem. Commun.* **2000**, *17*, 1671.
(12) Deckman, H. W.; Dunsmuir, J. H. *Appl. Phys. Lett.* **1982**, 377.
(13) Jensen, T. R.; Schatz, G. C.; Van Duyne, R. P. *J. Phys. Chem.* **1999**, 2394.
(14) Hilger, A.; Cuupers, N.; Tenfelde, M.; Kreibig, U. *Eur. Phys. J.* **2000**, 115.
(15) Haynes, C. L.; Van Duyne, R. P. *J. Phys. Chem. B* **2001**, *105*, 5599.
(16) Haynes, C. L.; McFarland, A. D.; Smith, M. T.; Hulteen, J. C.; Van Duyne, R. P. *J. Phys. Chem. B* **2002**, *106*, 1898.
(17) Haes, A. J.; Van Duyne, R. P. *J. Am. Chem. Soc.* **2002**, *124*, 10596.
(18) Micheletto, R.; Fukuda, H.; Ohtsu, M. *Langmuir* **1995**, *11*, 3333.
(19) Rakers, S.; Chi, L. F.; Fuchs, H. *Langmuir* **1997**, *13*, 7121.
(20) van Blaaderen, A.; Ruel, R.; Wiltzius, P. *Nature* **1997**, *385*, 321.
(21) Trau, M.; Saville, D. A.; Aksay, I. A. *Science* **1996**, *272*, 706.
(22) Yeh, S. R.; Seul, M.; Shraiman, B. I. *Nature* **1997**, *386*, 57.
(23) Heath, J. R.; Knobler, C. M.; Leef, D. V. *J. Phys. Chem. B* **1997**, *101*, 189.

10.1021/la0494674 CCC: $27.50
Published on Web 07/01/2004

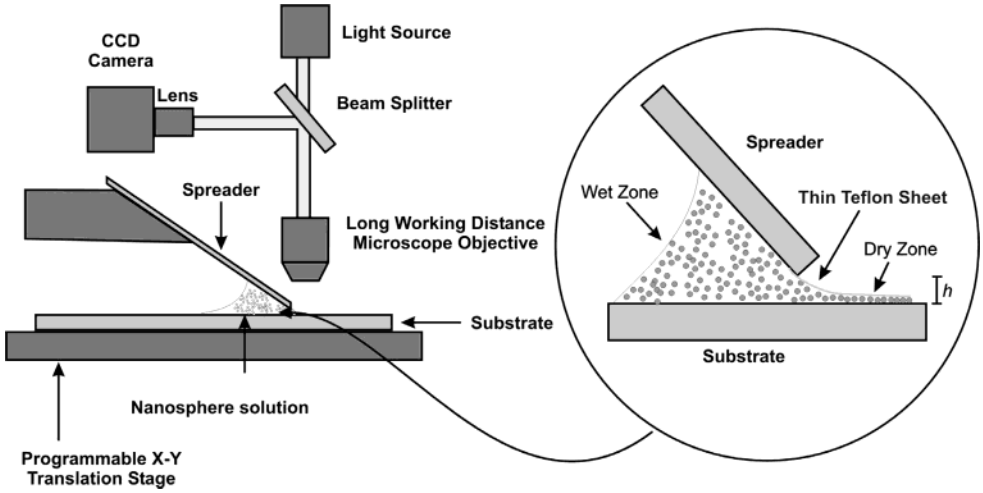

Figure 1. Depicted is a schematic diagram of the CSA apparatus. The expanded view shows the meniscus formation when the spreader is located at a position *h* above the substrate as well as the dry and wet zones critical to colloidal crystal formation.

size, shape, and interparticle spacing. The in-plane width and out-of-plane height of NSL-fabricated nanoparticles can be independently tuned, with nanometer precision, by selection of the nanosphere diameter used in the two-dimensional colloidal crystal deposition template and by the mass thickness of the material deposited.[15] Nanoparticle shape is controlled by the precision of the template, the angle of deposition,[24] or alternatively, by post-deposition processing steps such as thermal annealing. The particles and the templates have become the topic of a wide variety of studies because these colloidal crystals and nanoparticles can serve as etching masks to increase the efficiency of light-emitting diodes,[25] photonic band gap materials,[26−33] chemical and biological sensors,[17,34−39] and adhesive media[40,41] and even as calibration standards.[42]

The two-dimensional colloidal crystal template used in previous studies is fabricated by a suspension of nanospheres drop-coated onto the substrate where they self-assemble into a hexagonally close-packed array.[10] The colloidal crystal templates are then mounted into the chamber of a vapor deposition system where various thicknesses of Ag or Au can be deposited onto the surface. The formation of the hexagonally close-packed nanosphere arrays is the most critical step in NSL to produce highly ordered and uniform nanoparticles. Analogous with all natural crystals, disordered packing of the nanospheres results in point defects, slip dislocations, and grain boundaries.[10,43,44] However, the ability to controllably generate well-ordered, highly reproducible colloidal crystals of known dimensions is one of the greatest challenges to these types of studies. The additional constraint of monolayer formation for the two-dimensional crystals of NSL increases the difficulty of this problem.

In this work, we describe the development of a method based on convective self-assembly (CSA) of the nanospheres, which improves upon the drop-coating methods by decreasing the defect percentage within two-dimensional arrays. With this technique, it is possible to produce well-packed samples over a 1-cm^2 area. This method will be discussed, and the characterization of the final samples by the use of UV−visible extinction spectroscopy, atomic force microscopy (AFM), and scanning electron microscopy (SEM) will be shown. We will also discuss a new spectral mapping technique used to rapidly characterize entire samples.

Experimental Section

1. Materials. Ag (99.99%) was purchased from D. F. Goldsmith (Evanston, IL). Tungsten vapor deposition boats were purchased from R. D. Mathis (Long Beach, CA). Glass substrates were 18-mm-diameter, no. 2 coverslips from Fisher Scientific (Fairlawn, VA). Pretreatment of glass substrates required H_2SO_4, H_2O_2, and NH_4OH, all obtained from Fisher Scientific (Fairlawn, VA). Surfactant-free, white carboxyl-substituted polystyrene latex nanospheres with diameters of 390 ± 19.5 nm were received as a suspension in water from Duke Scientific (Palo Alto, CA). Absolute ethanol was purchased from Pharmco (Brookfield, CT).

2. Nanosphere Mask Formation by CSA. Figure 1 shows a schematic diagram of the CSA apparatus. The substrates, 18-mm square glass coverslips (Fisher Scientific, Pittsburgh, PA), were placed horizontally on a programmable translation stage (Newport, Irvine, CA), and a 10-mL drop of 4% (w/v) nanosphere solution of 400-nm-diameter carboxyl-functionalized polystyrene nanospheres (Interfacial Dynamics, Portland, OR) was placed onto the edge of the substrate. Using a thin Teflon sheet 1 mm in thickness, attached to a rectangular glass coverslip (Fisher Scientific, Pittsburgh, PA) placed at a distance, *h* (typically 0.001 mm), above the substrate surface, the solution was spread at a

(24) Haynes, C. L.; Van Duyne, R. P. *Nano Lett.* **2003**, *3*, 939.
(25) Windisch, R.; Dutta, B.; Kuijk, M.; Knobloch, A.; Meinlschmidt, S.; Schoberth, S.; Miesel, P.; Morghs, G.; Dohler, G.; Heremans, P. *IEEE Trans. Electron Devices* **2000**, 1492.
(26) Velev, O. D.; Jede, T. A.; Lobo, R. F.; Lenhoff, A. M. *Nature* **1997**, *389*, 447.
(27) Zhao, Y.; Avrutsky, I.; Li, B. *Appl. Phys. Lett.* **1999**, *75*, 3596.
(28) Winjnhoven, J. E. G. J.; Vos, W. L. *Science* **1998**, *281*, 802.
(29) Zakhidov, A. A.; Baughman, R. H.; Iqbal, Z.; Cui, C.; Khayrullin, I.; Dantas, S. O.; Marti, J.; Ralchenko, V. G. *Science* **1998**, *282*, 897.
(30) Yang, P.; Deng, T.; Zhao, D.; Feng, P.; Pine, D.; Chmelka, B. F.; Whitesides, G. M.; Stucky, G. D. *Science* **1998**, *282*, 2244.
(31) Subramania, G.; Constant, K.; Biswas, R.; Sigalas, M. M.; Ho, K. M. *Appl. Phys. Lett.* **1999**, *74*, 3933.
(32) Pan, G.; Kesavamoorthy, R.; Asher, S. A. *Phys. Rev. Lett.* **1997**, *78*, 3860.
(33) Burmeister, F.; Schafle, C.; Matthes, T.; Bohmisch, M.; Boneberg, J.; Leiderer, P. *Langmuir* **1997**, *74*, 22983.
(34) Bauer, G.; Pittner, F.; Schalkhammer, T. *Mikrochim. Acta* **1999**, 107.
(35) Storhoff, J. J.; Elghanian, R.; Mucic, R. C.; Mirkin, C. A.; Letsinger, R. L. *J. Am. Chem. Soc.* **1998**, 1959.
(36) Velev, O. D.; Kaler, E. W. *Langmuir* **1999**, *15*, 3693.
(37) Nayral, C.; Viala, E.; Fau, P.; Senocq, F.; Jumas, J. C.; Maisonnat, A.; Chaudret, B. *Chem.—Eur. J.* **2000**, 4082.
(38) Elghanian, R.; Storhoff, J. J.; Mucic, R. C.; Letsinger, R. L.; Mirkin, C. A. *Science* **1997**, 1078.
(39) Holtz, J. H.; Asher, S. A. *Nature* **1997**, *389*, 829.
(40) Garrett, J.; Lovell, P. A.; Shea, A. J.; Vinely, R. D. *Macromol. Symp.* **2000**, *151*, 487.
(41) Mayer, A.; Pith, T.; Hu, G. H.; Lambla, M. J. *J. Polym. Sci., Part B: Polym. Phys.* **1995**, *33*, 1781.
(42) Li, Y.; Linsday, S. M. *Rev. Sci. Instrum.* **1991**, 2630.
(43) Wei, Q. H.; Cupid, D. M.; Wu, X. L. *Appl. Phys. Lett.* **2000**, 1641.
(44) Dimitrov, A. S.; Miwa, T.; Nagayama, K. *Langmuir* **1999**, 5257.

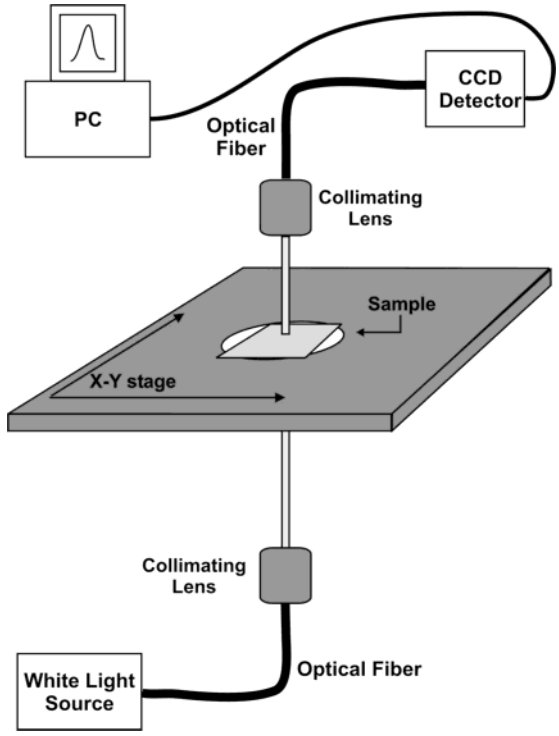

Figure 2. Depicted is a schematic diagram of the scanning UV−vis macro-extinction spectrometer used to obtain the image maps of a large area of Ag nanoparticles.

constant rate of 0.035 mm/s. The position of the spreader created two zones on the substrate surface. Monolayer formation occurs in the front, or dry, zone. The back, wet zone consists of the bulk of the solution droplet. Array growth was monitored using a 200-mm focal length lens (Mitutoyo, Japan) and a color charge-coupled device (CCD) camera (Sony, Tokyo, Japan). This allowed for rate changes and manipulation of other variables in situ to study their affects on sample quality. Humidity and temperature were not controlled and varied from 70 to 72 °F and 5−10% humidity.

3. Preparing Periodic Particle Arrays (PPAs). After the formation of the nanosphere template, the samples were mounted in a vapor deposition system (Consolidated Vacuum Corp., Rochester, NY). Ag (D. F. Goldsmith, Evanston, IL) was deposited at a rate of approximately 0.1 nm s^{-1} as measured by an XTM/2 deposition monitor quartz crystal microbalance (Leybold Inficon, East Syracuse, NY). After deposition, the nanosphere mask was removed via sonication of the sample in absolute ethanol (Pharmaco, Brookfield, CT) for approximately 2 min.

4. AFM. AFM images were collected using a Digital Instruments Nanoscope III microscope operated in tapping mode using etched Si nanoprobe tips (Digital Instruments, Santa Barbara, CA). These tips have resonance frequencies between 280 and 320 kHz and are conical in shape with a cone angle of 20° and an effective radius of curvature at the tip of 10 nm.

5. SEM. SEM images of the nanoparticle arrays were taken on a Hitachi S4500 Field Emission scanning electron microscope (Hitachi, Tokyo, Japan), with an accelerating voltage of 5 keV.

6. Scanning UV−Vis Macro-Extinction Spectroscopy. UV−vis extinction spectra were taken using white light (Ocean Optics, Dunedin, FL) transmitted through a 200-mm core multimode optical fiber. The light exiting the source fiber was focused onto the sample with a spot size approximately 0.5 mm in diameter using a collimating lens (Thor Labs, Newton, NJ). The light transmitted through the sample was collected with an identical collimating lens attached to the 200-mm core multimode fiber that was connected to a CCD camera (Ocean Optics, Dunedin, FL). Figure 2 shows a schematic diagram of this experimental arrangement. UV−vis extinction spectra were processed with a program written using Mathematica V4.0 (Wolfram Media, Champaign, IL).

Results and Discussion

Figure 1 depicts the experimental setup showing that the formation of a monolayer array is controlled by three processes: (1) capillary forces, which push the liquid from the bulk of the solution to the dry areas, (2) convective transfer of the nanospheres from the bulk of the solution to the thin wetting film, and (3) water evaporation.[45] When the solution drop is placed along the edge of the spreader, a pressure differential is created. This differential causes a capillary effect which transfers some of the solution from the bulk drop to the dry zone, forming a thin wetting film (expanded view Figure 1). When the evaporation begins, the nanospheres preferentially form a hexagonally close packed monolayer. To maintain this process, the stage is moved in the opposite direction to the monolayer formation at a constant velocity. The optimal velocity was found to be 0.035 mm/s to form a closely packed monolayer over a large section of the substrate. It is essential that the withdrawal rate be equivalent to the evaporation rate of the liquid in the dry zone for monolayer formation to occur. If the withdrawal rate is slower than the evaporation rate, nanospheres will accumulate and multilayer arrays (detrimental to NSL) will dominate the substrate surface. Conversely, rates of withdrawal in exceeding that of the evaporation rate will produce amorphous adsorption with multiple empty zones.

In addition to the rate control, the distance between the spreader and the substrate, h, also has an effect on the monolayer formation process. Control of h allows for regulation over the amount of bulk solution and the density of nanospheres in the solution that migrate from the wet zone to the dry zone. The addition of a thin Teflon membrane equalizes the capillary forces across the sample, which eliminates the need for extreme precision in the lateral placement of the spreader relative to the substrate. The high flexibility of the Teflon membrane prevented it from applying enough downward force onto the dry zone to disrupt film formation. Nitrogen was flowed in a direction perpendicular to the line of template formation to help keep the film drying time brief while pushing the nanospheres more tightly together.

The most prevalent method of evaluating the template quality produced by CSA is AFM imaging.[10,46] However, there are several severe limitations to this approach: (1) restricted access to sample sites, (2) unacceptable time, on the order of hours, required to resolve images from the large area of a sample, and (3) difficulty in distinguishing between monolayers, bilayers, and multilayers (Figure 3). Alternatively, an optical method of evaluation would eliminate these restrictions while allowing for quantitative evaluation of the samples. Ideally one would be able to monitor the optical properties of the bare nanospheres themselves. However, the spectra of two-dimensional arrays are very difficult to interpret as a result of diffuse scattering produced by defects in the packing arrangement of the colloidal template; therefore, the nanosphere template was used to create a PPA of Ag nanotriangles. The optical properties of Ag PPAs have been well-documented and provide a good starting point to test the performance of CSA. Utilization of the sensitivity of the LSPR is an excellent way to assess the quality and morphology of the nanosphere packing. Well-ordered CSA templates produce highly uniform PPAs with characteristic spectra, while poorly packed nanosphere templates do not. This difference can be used to characterize the

(45) Dimitrov, A. S.; Nagayama, K. *Langmuir* **1996**, *12*, 1303.
(46) Deckman, H. W.; Dunsmuir, J. H. *Fabrication of Microstructures over Large Areas. In Patent*; Exxon Research and Engineering Co.: Florham Park, NJ, U.S.A., 1987.

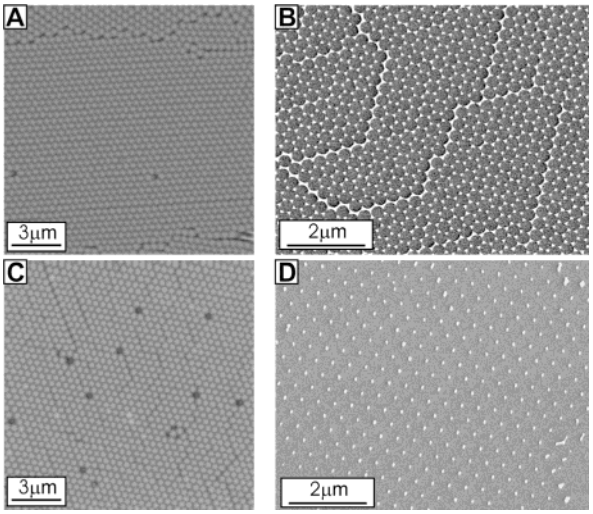

Figure 3. Comparison of AFM images of $D = 400$ nm nanospheres deposited onto a glass substrate with SEM images of the PPAs. Parts A and C correspond to tapping mode AFM images of bare nanosphere samples. Parts B and D correspond to SEM images of the samples after deposition of 50-nm Ag followed by nanosphere removal.

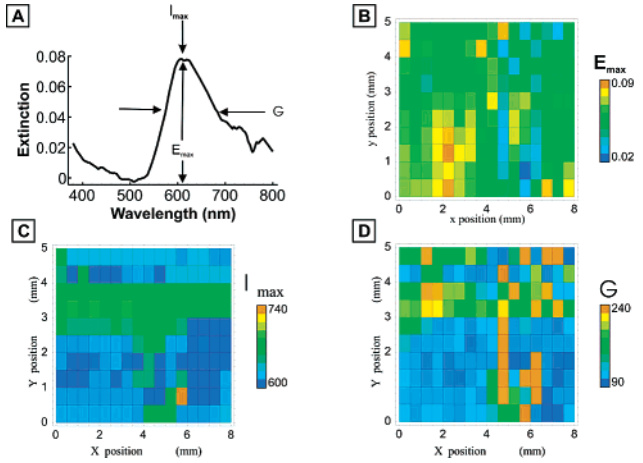

Figure 4. Shown are the UV−vis extinction spectroscopy and image maps of Ag nanoparticle arrays formed from nanospheres with $D = 400$ nm. Part A shows a representative single spectrum from the sample. Image maps: part B corresponds to E_{max}, C to λ_{max}, and D to Γ.

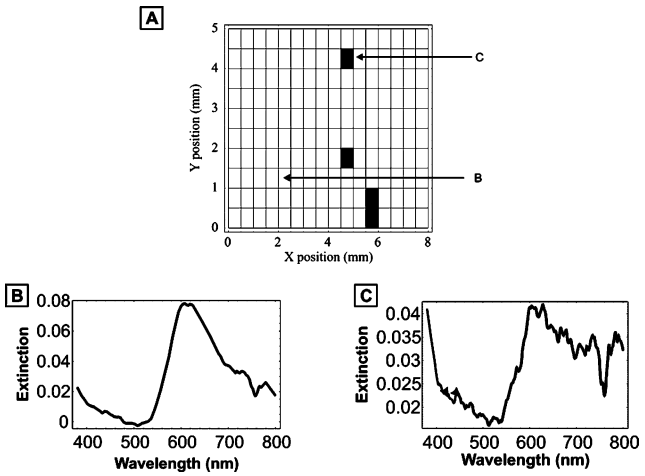

Figure 5. Shown are the UV−vis extinction spectroscopy and image map of Ag nanoparticle arrays. Part A shows a spatial plot of the data with restrictions applied for E_{max}, λ_{max}, and G. Spectra: B corresponds to a good pixel on the sample while C corresponds to a pixel that falls below the minimum requirements to be considered acceptable as a good-quality peak.

quality of each template produced. Figure 2 depicts the setup to be used to systematically analyze the LSPR across each sample.

For this study, 400-nm spheres were used to create the template for Ag deposition. The properties of PPAs formed by this template have been well-studied and well-documented, providing a good starting point in evaluating the quality of nanosphere templates formed by CSA. PPAs of different materials such as Au, Ni, and so forth can also be made but were not used in this study. The LSPR spectra of 50-nm Ag PPAs prepared using this template are known to have a maximum wavelength absorption peak(λ_{max}) at about 600 nm,[13] 0.1 absorbance units in magnitude (E_{max}) and 100-nm full-width at half maximum (G). Defects in the nanosphere mask, changes in packing morphologies, and insufficient or overabundant quantities of nanospheres result in defects in the metal nanoparticle array, which cause perturbations in the LSPR spectra. These perturbations in the spectrum do not produce information on the exact defect concentration in each sample. With each LSPR spectrum, the relative amount of defects can be obtained from the position and shape of the spectrum. A broad spectrum results from a large defect density, but the type and exact number cannot be obtained. Samples with a large shift in λ_{max} or extremely wide LSPR bandwidth are often associated with large Ag islands. A separate data file was created for each of the three important characteristics of the spectra. A single spectrum from the sample, shown in Figure 4A, confirmed that the sample exhibited the characteristic extinction peak for an array of 50-nm Ag nanoparticles prepared with a 400-nm sphere template. This extinction spectrum is an averaging of the many different plasmon resonances across the sample. With the use of scanning UV−vis spectroscopy gray-scale images, Figure 4B−D was generated of E_{max}, λ_{max}, and Γ, respectively, to monitor the plasmon resonance in smaller areas. In looking at these smaller areas, variations can be seen in each map. These variations are caused by the variations in packing across the sample giving rise to individual peak characteristics. Again the exact number of defects cannot be obtained with this characterization approach; however, the overall quality of each spot can be addressed on the basis of spectral shape, which can provide information on the relative amount of defects overall as compared to other positions or arrays. That is, sharper peaks are to be found in areas with fewer defects, whereas areas with more defects show distinct peak broadening. This means that the spectra are sensitive to defects within the spot size, but you cannot obtain the defect concentration.

While each individual peak characteristic is important, all three must be considered together when assessing the actual sample quality. Figure 5 is a spatial plot of the sample showing the area with acceptable plasmon resonance signals. An acceptable peak is defined as having (1) large E_{max} representing high signal-to-noise ratio, (2) reproducibility of λ_{max} (±20 nm for measurements in ambient conditions), and (3) Γ of 50−150 nm to eliminate noise peaks as well as those found in large absorption bands (as in the case of a Ag island). In the summation spectra shown in Figure 5, the white areas indicate locations of acceptable peaks while the black areas represent pixels outside of the applied restrictions. This summation spectrum allows for the determination of high-quality samples for use in additional studies, and additionally, it directs the experimenter to the sections of

a sample that are of the best quality and are most likely to produce high-quality results in future spectroscopic analyses.

Conclusion

In this work, we have demonstrated a modified technique to obtain a large area (1 cm^2) of hexagonally close-packed arrays of nanospheres. The experimental design allows control over the volume of solution, the rate of withdrawal, the height of the spreader relative to the substrate, and the portion of the substrate to be covered with solution. This technique can be applied to any substrate by adjusting the experimental parameters.[47] All of these factors are quantitative in nature and leave no room for discrepancies between samples.

The CSA-fabricated hexagonally packed nanospheres have been analyzed by the use of a new spectral technique. This scanning UV−vis spectroscopy allows for the analysis of large areas of the prepared sample in a reasonable time, with reproducible and reliable measurements. Future studies will be aimed toward adapting the current horizontal CSA apparatus to a vertical apparatus to obtain large areas of monolayers. In addition, the setup will be used to form colloidal crystals on new substrates and improve the overall sample quality under controlled temperature and humidity.

Acknowledgment. Funding for this work was provided by the ARO (Grant DAAG55-97-1-0133) and the MRSEC program of the NSF (Grant DMR-0076097). J.C. was funded by the CDCH-UCV (Grant 03.12.454999) and the CONICIT (Grant g-97000722). The authors would also like to acknowledge Mr. Michael Davis for initiating the CSA studies described herein.

LA0494674

(47) Rossi, R. C.; Lewis, N. S. *J. Phys. Chem. B* **2001**, *105*, 12303.